International Journal of Advanced Technology and Engineering Exploration, Vol 10(102)
ISSN (Print): 2394-5443 ISSN (Online): 2394-7454
http://dx.doi.org/10.19101/ IJATEE.2022.10100409

Research Article

Electrochemical equivalent circuit modeling using LTSPICE XVII for EGFET pH sensor based on TiO_2 sensing electrode experimental value

Shaiful Bakhtiar Hashim[1,3] Zurita Zulkifli[2*], Muhammad Alhadi Zulkefle[3] and Sukreen Hana Herman[3,4]
School of Electrical Engineering, College of Engineering, Universiti Teknologi MARA Cawangan Terengganu, 23000 Dungun, Terengganu, Malaysia[1]
Nano-Electronic Center, School of Electrical Engineering, College of Engineering, Universiti Teknologi MARA, 40450 Shah Alam, Selangor, Malaysia[2]
Integrated Sensors Research Group, School of Electrical Engineering, College of Engineering, Universiti Teknologi MARA, 40450 Shah Alam, Selangor, Malaysia[3]
Microwave Research Institute, Universiti Teknologi MARA, 40450 Shah Alam, Selangor, Malaysia[4]

Received: 11-November-2022; Revised: 23-May-2023; Accepted: 26-May-2023

Abstract
The design and simulation of an electrochemical equivalent circuit for an extended-gate field-effect transistor (EGFET)-based pH sensor was presented in this paper. The pH sensor is essential in various fields, such as biomedical applications, environmental monitoring, and industrial processes. The proposed sensor utilized the EGFET structure to measure pH with high sensitivity and precision. In this study, an electrochemical equivalent circuit was developed to model the EGFET pH sensor behavior. The circuit comprised various components, including resistors, capacitors, and voltage sources, representing the electrical characteristics of the pH sensor. The circuit was simulated using LTSPICE XVII, a widely-used electronic circuit simulator. Experimental values obtained from actual pH measurements are utilized to validate the accuracy of the proposed electrochemical equivalent circuit. The simulated results are compared against the experimental data to ensure the circuit accurately captured the behavior of the pH sensor. The simulation allowed for a detailed analysis of the sensor performance under different pH conditions and optimized the sensor design parameters. It was found that the experimental transfer and output characteristics of the EGFET were very similar to those from the simulation program with integrated circuit emphasis (SPICE) simulation, and gate-to-source voltage (VGS) value at 3 V exhibited the value of drain current, ID at 234.002 µA, which is similar to the transfer characteristic of CD4007UBE using semiconductor device analyzer (SDA). Other than that, the changes in value components in the equivalent circuit did not affect the transfer and output characteristics graph. Still, the capacitor value produced significant output variation in the simulation. This can be related to the modification on the equivalent circuit with additional voltage, source to bulk (VSB), to produce the different threshold voltage (VT) values at different pH.

Keywords
Electrochemical, Equivalent circuit, EGFET, LTSPICE XVII, pH sensor.

1.Introduction
An electrochemical sensor has gained significant attention due to its ability to translate ion analysis into an existing signal, potential difference, and impedance. This method is commonly used due to its simple operation, good sensitivity, easy miniaturization, and low power consumption. The technique has been used for in situ quantitative analysis and real-time monitoring of environmental parameters. It can be divided into three categories, voltammetric, impedimetric, and potentiometric, depending on the details of the experimental design [1–9]. For potentiometric, the electrostatic potentials (volt (V)) are measured and do not involve current in the measurement. While for voltammetric and impedimetric, current measurement is involved, and the electrode's potential was held or used as a variable input during measurement. While for voltammetric and impedimetric, current measurement is involved and the electrode's potential was held or used as a variable input during measurement.

*Author for correspondence

One of the sensors developed based on the electrochemical concept is the ion-sensitive field effect transistor (ISFET) sensor, usually associated with pH sensing. The basic configuration of ISFET is derived from a metal-oxide-semiconductor field-effect transistor (MOSFET), in which the metal gate is substituted by an ion-sensitive membrane with direct contact with a buffer solution [10]. However, the ISFET still suffers from several disadvantages, including device instability and poor sensitivity [11]. However, these disadvantages can be overcome by the extended-gate field effect transistor (EGFET) structure.

EGFET was proposed by Lauks et al. in 1983 [12]. EGFET structure isolated the field effect transistor (FET) from the chemical environment, in which a chemically sensitive membrane (or sensing electrode (SE)) was deposited at the end of the signal line extending from the FET gate electrode [13]. It offers several advantages, such as light insensitivity, simpler packaging, and flexibility for the shape of the extended gate area, as reported by [13–18]. EGFET has been applied in an extensive range of applications to detect any substance, especially as biosensors. EGFET is also favorable because it can be characterized using the simple connection and flexibility of the extended gate design [19].

Computer-aided design (CAD) tools have made the simulation of semiconductor-based devices possible before going through the complex fabrication process [20–23]. The CAD will reduce the cost and also the design cycle. A simulation program with integrated circuit emphasis (SPICE) is a CAD tool with built-in models for active devices like MOSFETs and bipolar junction transistors (BJTs). Martinoia et al. [24] introduced the first ISFET SPICE macromodel using a generalized SPICE model. They incorporated silanol and primary amine binding sites and evaluated device performance by modifying the model card of a metal oxide transistor. The model was used to study nonideal effects such as hysteresis and partial insensitivity to pH. The BIOSPICE model was further modified to incorporate transient dependence, and a thermal model was developed to account for temperature effects. The simulated results matched well with experimental studies of ISFET devices. However, the SPICE model's implementation was limited, with unavailable source code and complex compilation requirements. Then, the macromodel of ISFET in SPICE was further developed by Martinoia and Massobrio [25]. They came out with the original SPICE-2G and created BIOSPICE, which contains a built-in Physico-chemical model to deal with electrochemical devices such as ISFET-based sensors. Abu et al. [26] came out with an ISFET macromodel that contributed as a new subcircuit block for the LTSPICE component library to design ISFET-based sensors or microsystems. Unlike other authors, Kwon et al. [27] developed a macromodel for ISFET that addresses the issue of current drift. Their model represented the FET as two capacitors, one with a pure gate-oxide capacitance (C1) allowing slow movement of hydrogen ions and the other with a defective gate-oxide capacitance (C2), enabling relatively faster ion movement. The drift effect is represented by the movement of hydrogen ions in the defective oxide, denoted as R2, connected in parallel with C2. The current drift model included a series combination of the electrolyte resistance (R1) and a parallel combination of R2, C2, and C1. The model was experimentally validated using the transient current characteristics of a fabricated silicon nanowire pH sensor. The results demonstrated that the drift in the sensor is caused by the enhanced penetration of hydrogen ions through the defective oxide layer under the influence of an electric field.

Thus, the development and simulation of electrochemical equivalent circuits have been extensively explored for ISFET sensors [28–34], but the discussion on EGFET sensors has been relatively limited. This created a gap in knowledge and understanding, as EGFET sensors offer distinct advantages over their ISFET counterparts, including improved stability, sensitivity, and flexibility in design. The challenges in designing and simulating an electrochemical equivalent circuit for EGFET sensors using LTSPICE lie in capturing the complex electrochemical phenomena that occur at the interface of the SE and the solution. This involves considering various factors, such as ion selectivity, double-layer capacitance, charge transfer resistance, and diffusion processes.

So, this paper aims to study the equivalent circuit of the electrochemical method with an EGFET structure setup simulated using LTSPICE XVII by considering the fundamental electrochemical processes and incorporating experimental values. The simulation results obtained from the circuit model will facilitate optimizing the EGFET sensor design, enabling improved sensitivity, response time, and selectivity. In addition, based on the theoretical knowledge of the EGFET mechanism, the characteristic and relationship of resistor and capacitor representing SE and reference electrode (RE) were studied.

This paper is organized in several sections, starting with an introduction in Section 1, followed by a literature review in Section 2. Section 3 explains the design methodology for implementing the equivalent circuit, while Section 4 provides an in-depth analysis of the results. Section 5 discusses various characteristics and limitations. Finally, the paper concludes with Section 6.

2.Literature review

2.1Modeling and simulation setup

Most of the reported ISFET behavioral macromodel comprised two main stages: the electrochemical stage and the electronic stage [35, 36]. The electrochemical stage included the RE and the electrical double-layer capacitance, while the electronic stage involved an n-channel MOSFET. The equivalent circuit of an ISFET that represented the electrochemical and electronic stages was a capacitor, which was based on Fick's first law of diffusion, the Gouy-Chapman-Stern-Graham model, and the Shockley-Read-Hall model [37–39]. ISFET equivalent circuits use Fick's first law of diffusion describes the rate at which a substance diffuses through a medium, which may apply to the ISFET's solution ions. This law compensates for the sensor's ion diffusion processes in the circuit model. The Gouy-Chapman-Stern-Graham model also affects ISFET equivalent circuit representation. This model describes ion behavior at the solid-solution interface. The electrical double layer at the solid surface and ion-charged surface interaction is considered. This model highlights the ISFET's sensing interface electrochemical processes when added to the circuit. In semiconductor physics, the Shockley-Read-Hall model describes charge carrier recombination and generation. It incorporates semiconductor material imperfections or impurities that modify charge flow. The ISFET's equivalent circuit addresses electronic stages and charges carrier behavior in the transistor structure by including this model. In general, the integration of different scientific models into the equivalent circuit depiction of an Ion-sensitive field effect transistor (ISFET). The circuit aims to capture the electrochemical and electronic processes involved in the functioning of the ISFET by utilizing Fick's first law of diffusion, the Gouy-Chapman-Stern-Graham model, and the Shockley-Read-Hall model. The detailed circuit diagram aids in comprehending the sensor's actions and simplifies the process of analyzing and interpreting its readings [31] and [40–42].

Thus, this paper used the basic configuration of potentiometric measurement, as shown in *Figure 1*. The basic configurations consist of RE and ion-selective electrodes (ISE), which convert a particular ionic activity to a specific potential. The potentiometric measurement measures the voltage difference between RE and ISE when both electrodes are dipped in the same buffer solution or electrolyte. The characteristic of ISE controls the ionic activity called response and can be related to the Nernst equation, as shown in Equation 1[43].

$$E(T) = E^{o}(T) - 2.303\,RT/nF\,pH \qquad (1)$$

Where,

E(T)=Measured potential mV at temperature T (Kelvin)
$E^{o}(T)$=Constant, standard potential mV at temperature T (Kelvin)
2.303 = Factor to convert ln to log
R=Molar gas constant (8.3144 J mol^{-1} K^{-1})
F= Faraday constant 96485 C mol^{-1}
T= Temperature K (kelvin)

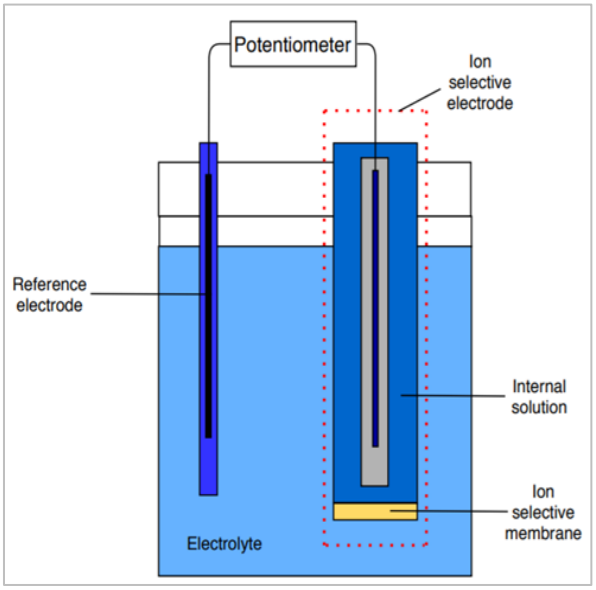

Figure 1 The basic configuration of the potentiometric measurement

The Nernst equation is a mathematical description of an ideal pH electrode in electrochemistry [44]. It can accurately predict cell potentials only as the equilibrium quotient is expressed in activities. The sensor is considered good if the sensitivity value is near the theoretical Nernstian value of 59.20 mV/pH and the linearity value is near 1.

Figure 2 shows the potentiometric equivalent circuit consisting of resistors and capacitors. By referring to *Figure 2*, the resistor (R_{REF}) and capacitor (C_{REF}) in parallel represent the RE, and the resistor (R1) and capacitor (C1) in parallel represent the ISE. In contrast, the resistor (Rs) in series between the two parallel components represents the buffer solution or electrolyte. The value of the potential difference between RE and ISE at different solution buffers is measured by a voltmeter (V).

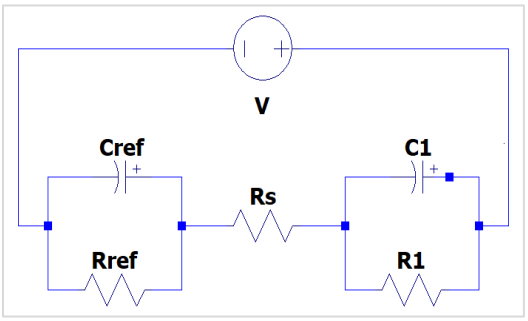

Figure 2 Potentiometric equivalent circuit

The capacitor components in this equivalent circuit can be described with the Helmholtz double layer, which represents the accumulation of electrical charges present at the boundary of an electrode and electrolyte when they are in contact with each other as in *Figure 1*. The arrangement of positive and negative charges at the surface of the electrode leads to the capacitive behavior of charge storage [44]. While the resistor's role is to oppose the electrical current through it. This is called the resistance of electricity, which is measured in the ohm unit. The capacitance (C) and resistance (R) relationship are shown in Equation 2 and Equation 3;

$$C = q/V \quad (2)$$

$$R = V/I \quad (3)$$

Where,
C = capacitance of the capacitor, Farads (F)
q = charge stored, Coulombs (C)
V = voltage, Volts (V)
R = resistance, Ohms (Ω)
I = current, Amperes (A)

2.2Electrochemical equivalent circuit

Figure 3 shows the experimental EGFET measurement setup. The RE was connected to a semiconductor device analyzer (SDA) Keysight B1500A, while the SE was connected to the gate of a commercialized MOSFET CD4007 as the extended gate SE.
This MOSFET is well documented in terms of width and length in the SPICE model, and the connectivity of this MOSFET is also versatile. The transfer and output characteristics were obtained from this measurement setup.

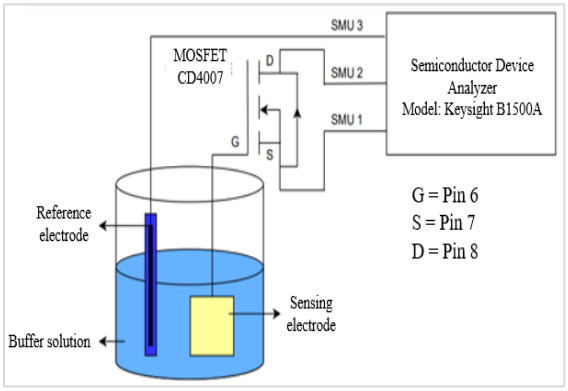

Figure 3 EGFET measurement setup

Figure 4 shows the internal schematic circuit of CD4007 MOSFET. The CD4007 consists of 3 pairs inverter with pin 14 as a P-type metal oxide semiconductor (PMOS) and pin 7 as an N-type metal oxide semiconductor (NMOS). This inverter shares a common pin gate (6, 3, and 10). Pins 6, 7, and 8 were used for this measurement. Other pins (3, 4, 5, 10, 9, and 12) also can be used for measurement setup.

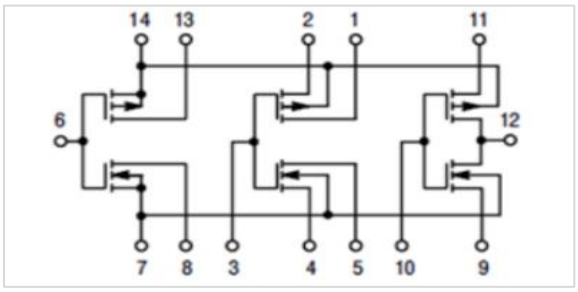

Figure 4 Schematic circuit CD4007 MOSFET

The EGFET equivalent circuit as shown in *Figure 5*, has been constructed by considering the potentiometric equivalent circuit (*Figure 2*). The difference between *Figure 2* and *Figure 5* is, *Figure 5* has additional NMOS MOSFET representing CD4007 that gate connected to sensing capacitor (C1) and resistor (R1) while reference voltage, V_{REF} connected to reference capacitor (C_{REF}) and resistor (R_{REF}).

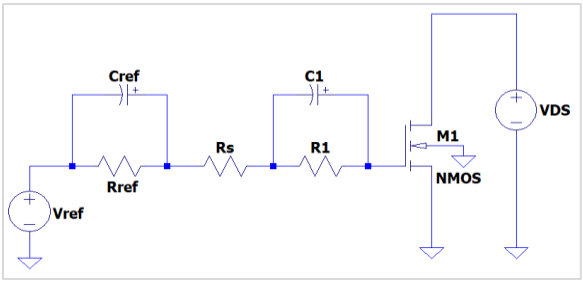

Figure 5 EGFET equivalent circuit

Figure 6 shows the basic reaction on metal oxide surface producing surface potential at (a) neutral, (b) acidic, and (c) alkaline conditions. As shown in *Figure 6*, the surface of metal oxide has a hydroxyl group and these hydroxyl groups are capable of interacting with pH potential determining ions (PDI) which are hydrogen ions (in an acidic solution) and hydroxide ions (in a basic solution). Depending on the type of PDI that is dominant in the solution, the surface of the sensing membrane will be either more positively or negatively charged. This positive and negatively charged can be represented by the capacitor C1 in EGFET equivalent circuit (*Figure 5*). The change of ion is detected based on the changes in capacitance. Therefore, the capacitance shall determine the amount of charge that can be adsorbed on the capacitor. In EGFET equivalent circuit, resistors RREF and R1 act as the charge transfer resistance and RS is the solution resistance.

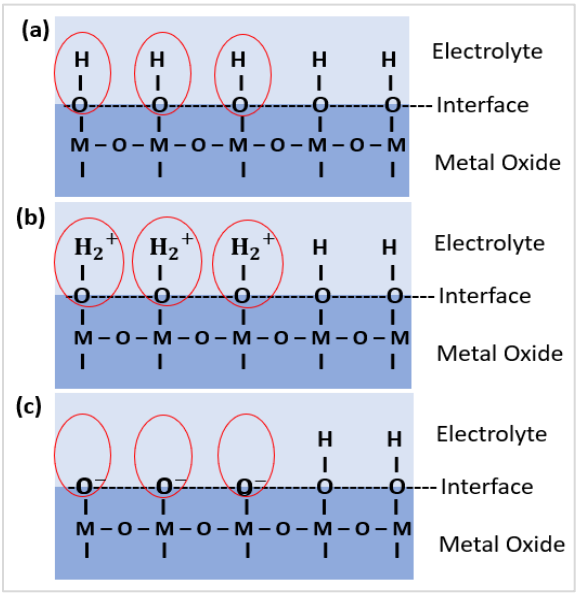

Figure 6 Basic reaction on metal oxide surface producing surface potential at (a) neutral, (b) acidic, and (c) alkaline conditions

3.Methodology

3.1Simulation of EGFET equivalent circuit

Figure 7 shows a block diagram representation flow of this project. This block diagram demonstrates the sequential process of arranging discrete components involving a resistor and capacitor connected to MOSFET, setting up MOSFET parameters, and simulating the I_D versus V_{GS} graph for an equivalent EGFET circuit. Each step contributes to the overall understanding and analysis of the circuit's functionality and performance.

Thus, in this simulation part, LTSPICE XVII was used to simulate the EGFET equivalent circuit and studied each component's characteristics and relationship to the current-voltage (I-V) characteristic. Before running the simulation, CD4007 MOSFET was modeled by setting up the parameters of the MOSFET, such as width (W), length (L), transconductance (K), lambda (λ), and $V_{T,}$ as shown in *Table 1*. This model was selected to compare with the simulation and experimental results.

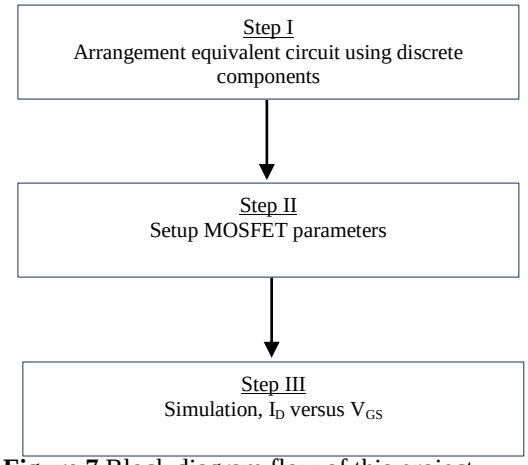

Figure 7 Block diagram flow of this project

Table 1 MOSFET parameters for LTSPICE simulation

Mosfet Parameters	Value
WIDTH (W)	170 µm
LENGTH (L)	10 µm
TRANSCONDUCTANCE (K)	74.33×10^{-6} S
LAMBDA (λ)	0.01
THRESHOLD VOLTAGE (V_T)	1.1

Figures 8 and *9* show the experimental output and transfer characteristics of CD4007UBE MOSFET, respectively, measured using SDA. The drain-to-source voltage (V_{DS}) value varied from 1 to 3 V and V_{GS} was fixed at 2V for output characteristics. While for transfer characteristics, V_{GS} was varied from 1 to 3 V, and V_{DS} was set at 100 mV.

As shown in *Figure 8*, there are three state regions: triode, linear, and active. When the V_{DS} is smaller, the CD4007UBE operates in the triode region. In this mode, the drain current is directly proportional to V_{DS} and can be described using Ohm's Law.

As a result, the characteristic output curve in the triode region slopes upward, demonstrating a linear relationship between I_D and V_{DS}. While in the saturation region or linear region, the V_{DS} is sufficiently large, causing the CD4007UBE to operate in saturation mode. In this mode, the drain current remains relatively constant regardless of further increases in V_{DS}. As a result, the characteristic output curve appears flat in the saturation region, indicating high current stability. These regions represent by the given formula as shown in Equation 4, Equation 5, and Equation 6 as follows:

$$I_D = \mu_n C_{ox} W/L\,(V_{GS} - V_t)V_{DS;\,\text{Triode region}} \quad (4)$$

$$I_D = \mu_n C_{ox} W/L\,[(V_{GS} - V_t)V_{DS} - V^2{}_{DS}/2];\ \text{Linear region} \quad (5)$$

$$I_D = 1/2\,\mu_n C_{ox} W/L\,(V_{GS} - V_t)^2;\ \text{The active region} \quad (6)$$

$$K = \mu_n C_{ox};\ \text{Transconductance}$$

Where I_D is the drain current, μ_n is the mobility, C_{ox} is the oxide capacitor, W is width, L is length, V_{GS} is the gate-source voltage, V_{DS} is the drain-source voltage, and V_T is the threshold voltage.

Three formulas represent three conditions from *Figure 8*: cut-off, linear, and saturation regions. In summary, the linear, active, and triode regions describe different modes of operation for a FET and the corresponding relationship between the voltage applied to the transistor and the resulting current flowing through it.

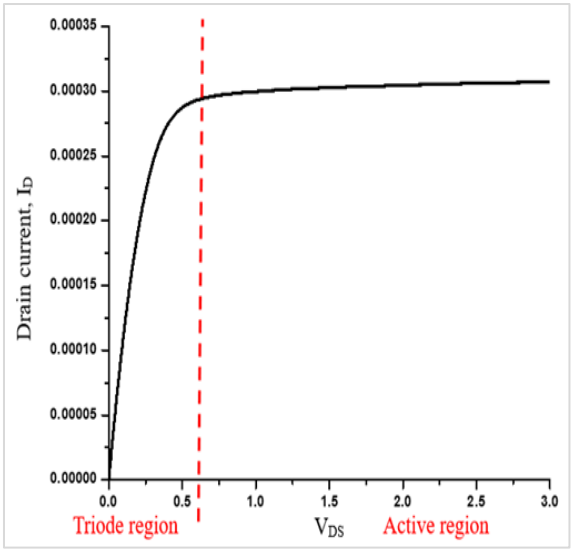

Figure 8 Output characteristic (I_D versus V_{DS}) of CD4007UBE using Semiconductor Analyzer

Equation 7, Equation 8, and Equation 9 describe the condition, respectively. The cut-off region where V_T is less than or equal to V_{GS}. The transistor is in an off state in the cut-off region, meaning there is no significant current flow between the source and drain terminals. This occurs when the applied V_{GS} is lower than the V_T of the transistor. The transistor acts as an open switch in this region, and the I_D is nearly zero. While for a linear region, V_{GS} greater than V_T. In this region, the transistor behaves as a voltage-controlled resistor.

The V_{GS} applied is higher than V_T, resulting in a conducting channel between the source and drain. The I_D increases linearly with V_{GS}, following Ohm's Law. The drain current is directly proportional to the V_{DS} as long as V_{DS} is not excessively large.

As shown in *Figure 9*, the value of V_T was around 1.1 V, and at V_{GS} 3 V. The value of I_D was around 234 µA. W and L values were assumed and fixed to 170 µm and 10 µm, respectively. The value of λ was also assumed to be 0.01. *Figure 10* shows the EGFET equivalent circuit with parameters.

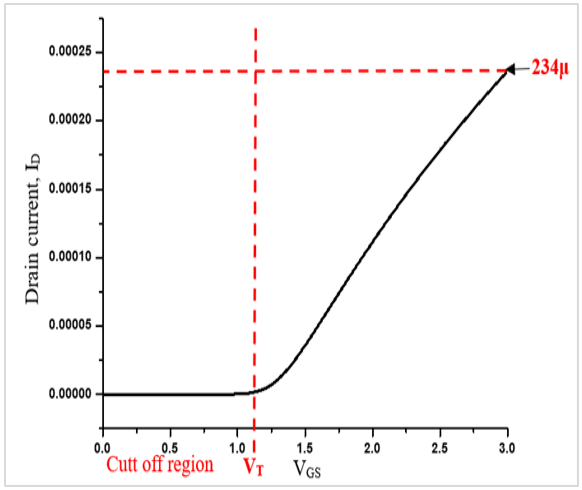

Figure 9 Transfer characteristic (I_D versus V_{GS}) of CD4007UBE using Semiconductor Analyzer

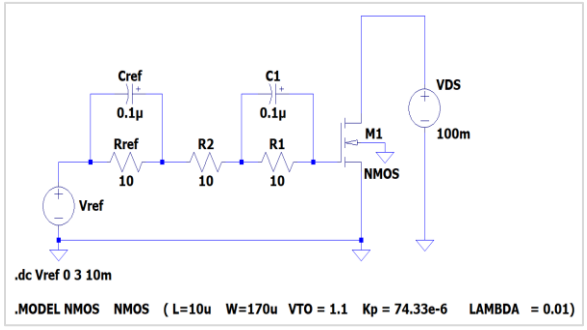

Figure 10 EGFET equivalent circuit with parameters

$$I_D = 0; V_{GS} \leq V_T \text{ ; Cut Off} \quad (7)$$

$$I_D = K\,W/L\left[(V_{GS} - V_t)V_{DS} - {V_{DS}}^2/2\right](1 + \lambda V_{DS}); V_{GS} > V_T, V_{DS} \leq V_{GS} - V_T; \text{ Linear region} \quad (8)$$

$$I_D = K\,W/L\,(V_{GS} - V_t)^2(1 + \lambda V_{DS});\ V_{GS} > V_T\ V_{DS} > V_{GS} - V_T \text{Saturation region} \quad (9)$$

By referring to Equation 7, the value of V_{GS} (3 V) is greater than V_T (1.1 V), and in the other condition, the value of $V_{GS} - V_T$ (3-1.1) is greater than V_{DS} (100 mV). Based on these conditions, the value of transconductance, K, can be calculated using the formula and found to be 74.33µ. Therefore, all these parameters W (170 µm), L (10 µm), K (74.33 µS), V_T (1.1 V), and lambda (0.01) were set in LTSPICE simulation as shown in *Figure 9*.

In this paper, the simulation was carried out for I_D versus V_{GS} at fixed V_{GS} at 3V, and I_D versus V_{DS} for V_{GS} fixed at 2V, with different capacitor and resistor values. The simulations involved using various capacitor and resistor values, which suggests that the study aimed to analyze the impact of varying circuit components on the behavior of the MOSFET. Other than that, the output current for variation of equivalent circuits, input and output characteristics at different pH levels, and input and output characteristics for different V_{REF} also were studied.

4.Results

4.1Graph analysis on simulation and experimental

Figures 11 and 12 are the I_D versus V_{GS} and I_D versus V_{DS} for EGFET equivalent circuit parameters for this simulation part. These parameters are defined based on the EGFET model and are represented in *Figure 10*. Specifically, *Figure 11* shows the output characteristic obtained through measurements using an SDA. *Figure 11* indicates that the I_D at a V_{DS} of 2V is measured to be 307 µA. However, it is observed that the simulation shows a higher value of I_D at 2V, measuring over 500 µA. This discrepancy between the measured and simulated values indicates a difference between the actual device behavior and the model used in the simulation.

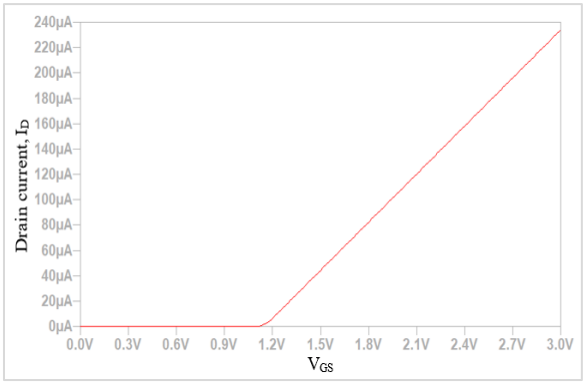

Figure 11 Simulation ID versus VDS graph at VREF 2V

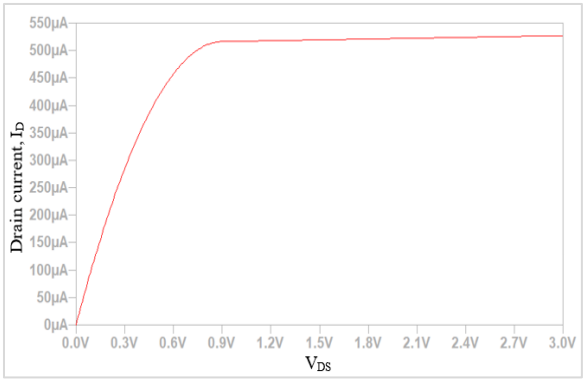

Figure 12 Simulation I_D versus V_{GS} graph

The value of I_D closed to 307 µA when the V_{GS} value at 1.8 V. So, it can be said that the simulation part and the actual are set to be in the same condition. Even though I_D values are slightly different between simulation and using SDA, this value is acceptable. *Figure 12* shows that V_{GS} at 3 V exhibited the value of I_D at 234.002 µA, which is similar to the transfer characteristic of CD4007UBE using SDA. The alignment between the simulated and actual conditions is crucial because it validates the accuracy and reliability of the simulation model. Furthermore, closely matching the simulated and actual results demonstrates that the simulation model accurately represents the circuit's behavior in real scenarios.

4.2Graph analysis on the reference and sensing electrode equivalent circuit

In this part of the simulation, each component C_{REF}, R_{REF}, R2, C1, and R1 was varied from low to a high value to observe the output changes in the I_D versus V_{GS} graph. The resistor was varied from 10 Ω to 1000 kΩ, while for capacitor was varied from 0.1 µF to 4700 µF. This indicates that different values were assigned to these components to assess the impact on the circuit's behavior, specifically the I_D versus V_{GS} relationship. By varying these components, the simulation can explore a range of possible circuit configurations and observe how these variations affect the output characteristics. Observing the output changes in the I_D versus V_{GS} graph makes it possible to identify trends, patterns, and relationships between the component values and the resulting drain current. This analysis can provide insights into the circuit's performance, its sensitivity to component variations, and the range of values that yield desirable or optimal operation. *Table 2* shows the current I_D output when the component's value in the EGFET equivalent circuit was changed. The simulation results showed no changes in the drain current for the different values of R and C. This implies that altering the values of R and C did not significantly impact the drain current in this particular circuit. Therefore, due to no changes for each component, R2 has been replaced with the voltage source, $V_{R2,}$ by assuming the voltage source act as potential differences between the two electrodes, as shown in *Figure 13*. A voltage source can manipulate the circuit behavior and potentially influence the I_D current. As shown in *Table 3*, as the value of V_{R2} increases, the I_D also increases. It shows that the potential difference at V_{R2} may result in different output values indicating a clear correlation between the potential difference at V_{R2} and the output values of I_D. This situation obeys Nascimento and Mulato [45], in which there are potential differences between RE and SE. That the ions in the solution are eventually attached to the sensor's surface due to their affinity with these ions. Consequently, the voltage value will change according to a different solution and sensing film, then the result will lead to an extra variable potential ΔV between the bulk solution and the film's surface.

Table 2 Summarize output for each component

		Reference Electrode(RE)			Sensing Electrode(SE)		Output
V_{REF} (V)	V_{DS} (mV)	C_{REF}	R_{REF}	R2	C1	R2	I_D/V_{GS} (µA)
3	100	0.1µ	10	10	0.1µ	**10-1000k**	234.002
3	100	0.1µ	10	10	**0.1-4700µ**	10	234.002
3	100	0.1µ	10	**10-1000k**	0.1µ	10	234.002
3	100	0.1µ	**10-1000k**	10	0.1µ	10	234.002
3	100	**0.1-4700µ**	10	10	0.1µ	10	234.002

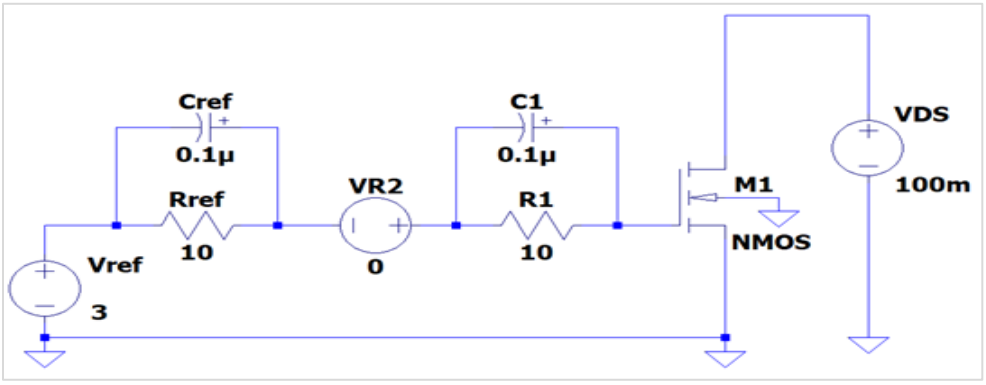

Figure 13 EGFET equivalent circuit with R2 changed to voltage V_{R2}

Table 3 Summarize output for different V_{R2}

		Reference electrode			Sensing electrode		Output
V_{R2} (V)	V_{DS} (mV)	C_{REF}	R_{REF}	R2	C1	R2	I_D/V_{GS} (A)
0	100	0.1µ	10Ω	10Ω	0.1µ	10Ω	234.00µ
1	100	0.1µ	10Ω	10Ω	0.1µ	10Ω	360.85µ
2	100	0.1µ	10Ω	10Ω	0.1µ	10Ω	486.97µ
3	100	0.1µ	10Ω	10Ω	0.1µ	10Ω	613.46µ
4	100	0.1µ	10Ω	10Ω	0.1µ	10Ω	739.95µ
5	100	0.1µ	10Ω	10Ω	0.1µ	10Ω	866.44µ
6	100	0.1µ	10Ω	10Ω	0.1µ	10Ω	992.93µ
7	100	0.1µ	10Ω	10Ω	0.1µ	10Ω	1.119m
8	100	0.1µ	10Ω	10Ω	0.1µ	10Ω	1.246m
9	100	0.1µ	10Ω	10Ω	0.1µ	10Ω	1.372m
10	100	0.1µ	10Ω	10Ω	0.1µ	10Ω	1.499m

Figure 14 (a)-(d) shows different configurations of the EGFET equivalent circuit to observe if there are any changes in the I_D versus V_{GS} graph. *Figure 14 (a)* is the same as *Figure 9*, *Figure 14 (b)* shows that all capacitors and resistors have been removed, while *Figure 14 (d)* only capacitor and resistor for the reference electrode part, and *Figure 14 (c)* capacitor and resistor for reference part as well as resistor R2. By depicting different circuit configurations, it aims to explore the effects of these variations on the behavior of the I_D versus V_{GS} relationship. Each configuration likely involves modifications to specific components or connections within the circuit, potentially influencing its overall performance.

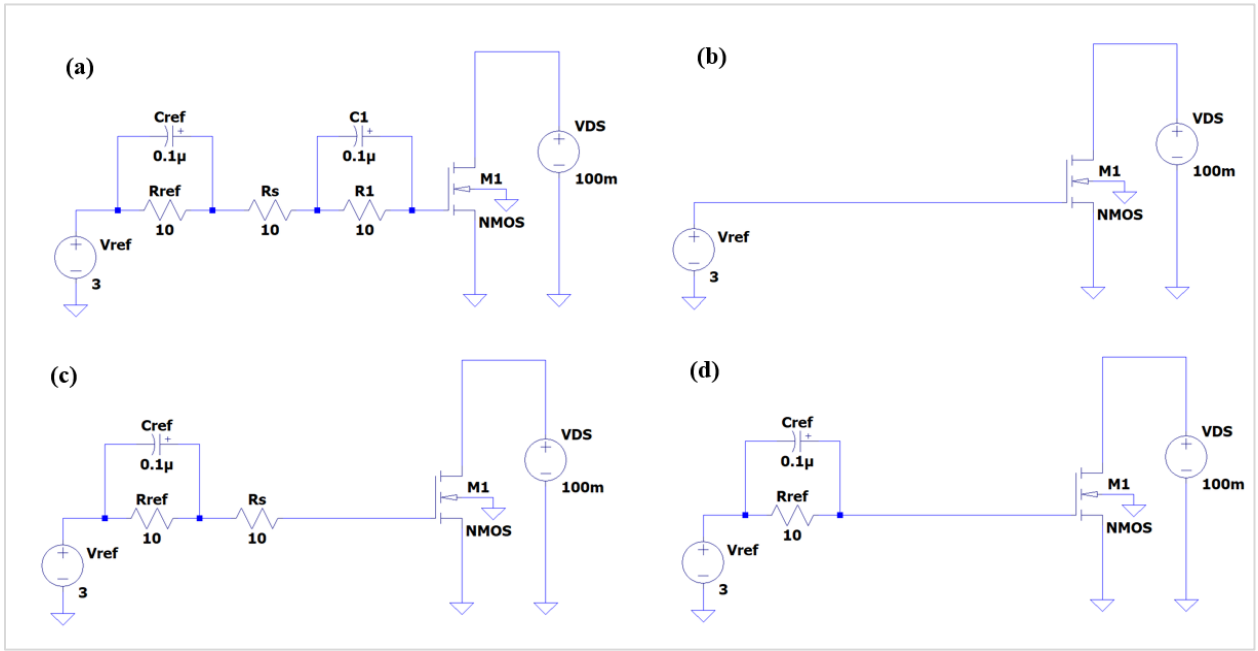

Figure 14 (a)-(d) EGFET equivalent circuit with R2 changed to voltage VR2

However, the simulation result shows the output for all equivalent circuits exhibited in the same graph where the value of I_D equals 234.002 µA. But a notable change occurred when a capacitor was added in series with R2 (as depicted in *Figure 15*). The output graph in *Figure 16* indicated an output of 209 fA. This means that the presence of the capacitor significantly reduced the current. Furthermore, the simulation was conducted with a fixed V_T value of 1.1V. Interestingly, the output current remained very small at 209 fA and was unaffected by changes in V_{GS}. However, when the V_T value was changed to 0V, the output characteristic exhibited an exponential curve, as shown in *Figure 17*. This suggests that the I_D current gradually increased as the VGS value increased from 0 to 3V.

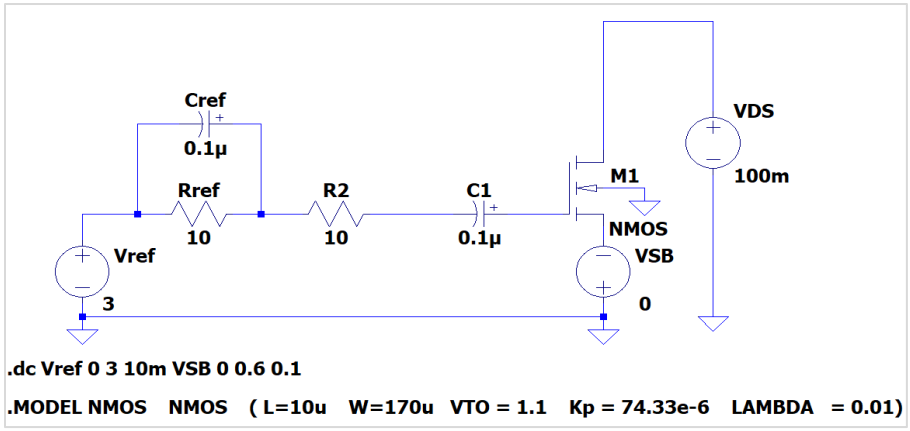

Figure 15 Equivalent circuit with single capacitor C1

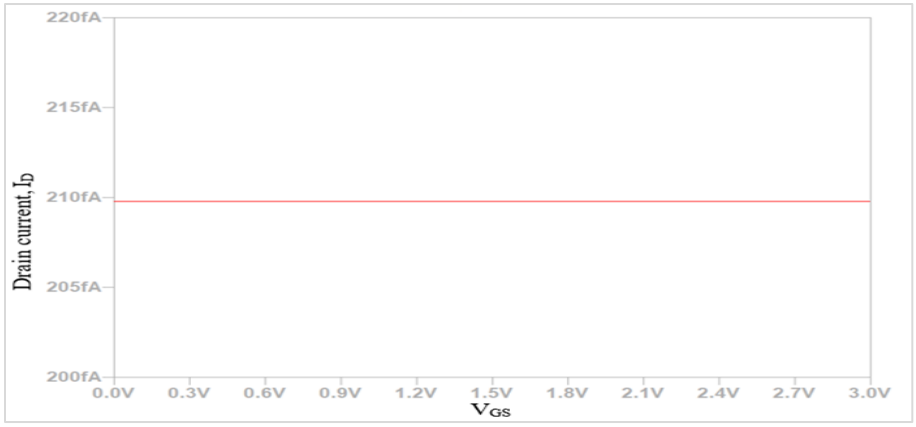

Figure 16 I_D versus V_{GS} graph for single capacitor C1

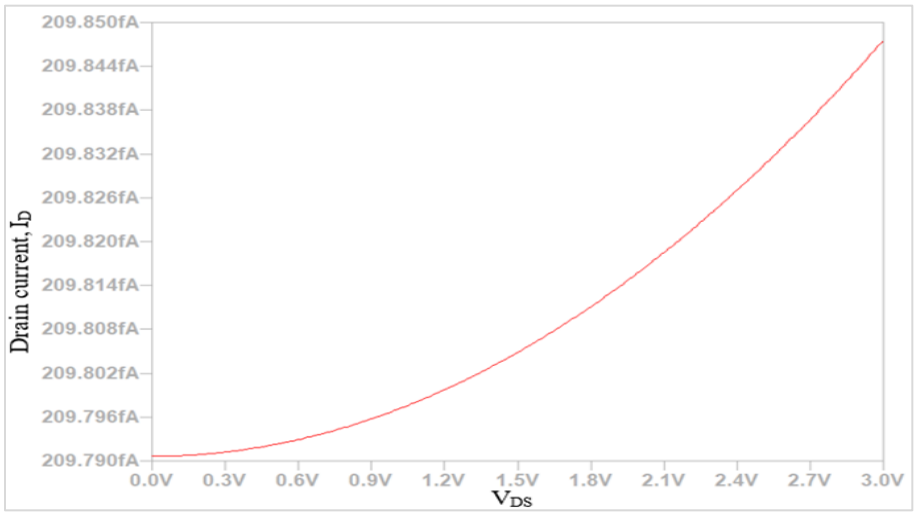

Figure 17 I_D versus V_{GS} graph with V_T equal to 0 V

4.3Comparison of SPICE simulation and experimental results

Figure 18 and *Figure 19* show the output and transfer characteristics measured by SDA with EGFET setup at different pH values (pH 2, 4, 6, 7, 8, 10, and 12) using titanium dioxide (TiO_2) SE data. The output characteristic shows that the I_D decreased as the pH value increased and that low pH yields a high I_D.

There is an inverse relationship between the pH value and the drain current. Additionally, it shows that low pH levels lead to higher drain currents. The drain current indicates this sensitivity, with higher currents indicating lower pH values and lower currents indicating higher pH values. This behavior is significant because it can be utilized for pH sensing applications or other relevant fields where pH detection is important.

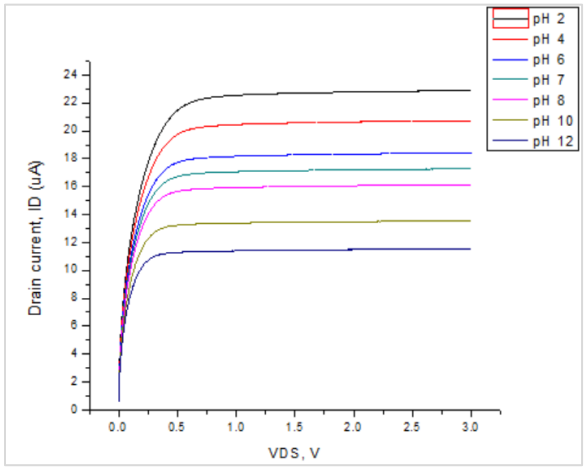

Figure 18 Experimental I_D versus V_{DS} graph at different pH values

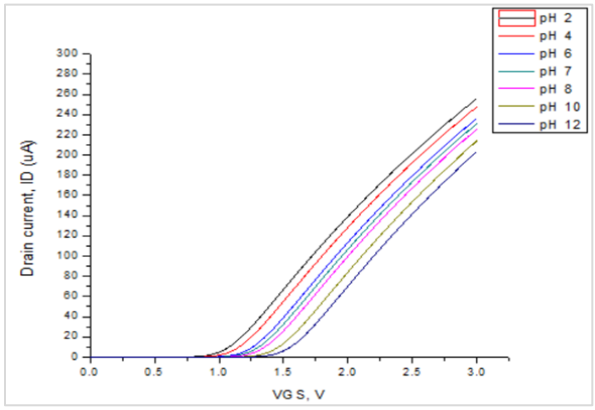

Figure 19 Experimental I_D versus V_{GS} graph at different pH values

Figure 20 displays a graph that represents the relationship between I_D and V_{DS} under different V_{REF} values. The graph was generated through LTSPICE simulation, utilizing an equivalent circuit shown in *Figure 10*. The pattern observed in *Figure 20* is similar to that of *Figure 18*, indicating that the drain current decreases as the pH value increases. The specific data points on the graph indicate that at pH 12, the drain current is approximately 500 µA, while at pH 2, it is around 50 µA. The graph illustrates a linear and proportional relationship between I_D and V_{DS} until I_D reaches saturation. At this point, the drain current remains constant for each pH value. *Figure 21* presents the graph depicting the relationship between I_D and V_{GS} under different V_{DS} values obtained through LTSPICE simulation. It is observed that the I_D varies with the V_{DS} value. However, the initial V_T remains consistent across all pH values. These findings diverge from the characteristics obtained in the experimental work, indicating the necessity for modification of the equivalent circuit.

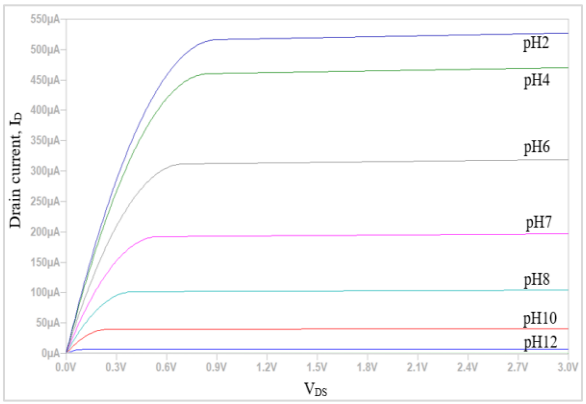

Figure 20 Simulation I_D versus V_{DS} graph at different V_{REF} values

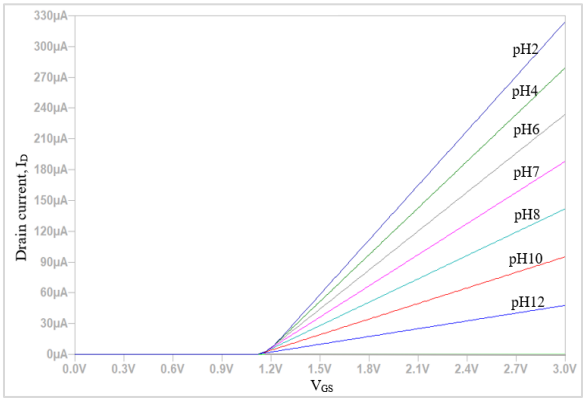

Figure 21 Simulation I_D versus V_{GS} graph at different V_{DS} values

Figure 22 illustrates the modified equivalent circuit with additional voltage, V_{SB}. The introduction of V_{SB} in the equivalent circuit significantly impacts the relationship between the I_D and the V_{GS}. The V_{SB} voltage affects the V_T of the transistor, which in turn influences the transistor's behavior in response to changes in V_{GS}. When V_{SB} is present, it creates a voltage difference between the transistor source and

the body, leading to the body effect. This voltage difference modifies the effective V_T and alters the transistor's turn-on and turn-off characteristics. Regarding the drain current versus V_{GS} relationship, the Body effect caused by V_{SB} introduces a second-gate control mechanism. The body, acting as a secondary gate, affects the effective gate voltage seen by the transistor. As a result, the transistor's behavior in terms of current flow and switching behavior is influenced by both the V_{GS} and the V_{SB} voltage [46].

By varying the V_{SB} and fixing the value of other components, it shows the different values of I_D at different values of V_T were obtained as shown in *Figure 23*. For example, at lower pH 2, the value of V_T was around 5.5 V; for pH 12 the value of V_T was around 1.15 V, which is a similar pattern to the experimental results.

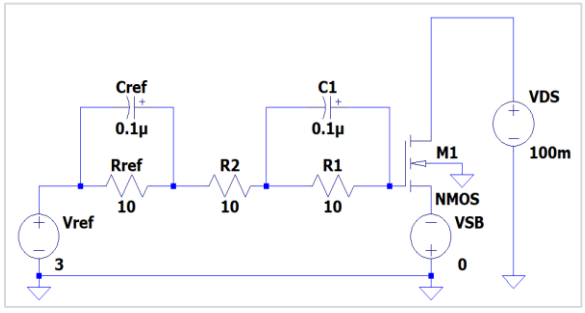

Figure 22 Modified equivalent circuit with additional voltage, V_{SB}

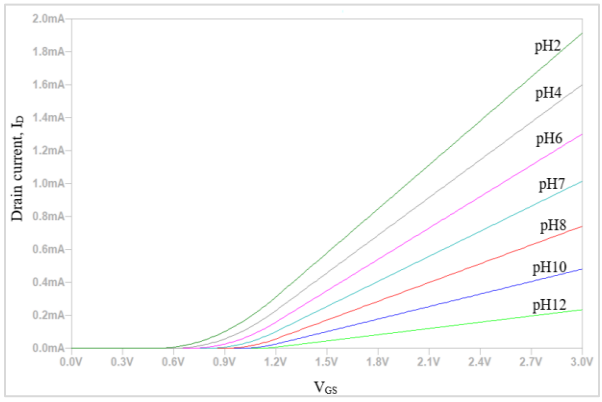

Figure 23 Simulation graph with varying V_{SB}

5.Discussion

This study focuses on simulating the EGFET equivalent circuit and various types of equivalent circuits using LTSPICE XVII with discrete components. The accurate modeling and simulation achieved in this research hold the potential to contribute significantly to the prediction of output current based on different pH levels. The results indicate a close resemblance between the simulation graph of transfer characteristics and the SDA. However, a slight disparity is observed in the output characteristic graph, particularly in terms of the drain saturation current value. Notably, the resistor and capacitor values in the equivalent circuit exhibit negligible influence on the transfer and output characteristics. Conversely, parameters associated with the MOSFET, such as width, length, transconductance, and threshold voltage, play a vital role in determining device behavior. Furthermore, the inclusion of the modified equivalent circuit with an additional voltage, V_{SB}, results in varying V_T values corresponding to different pH levels, which aligns with the experimental findings.

In addition, the study ensures a more realistic representation of the circuit by employing discrete components in the simulation. This contributes to the advancement of pH-based current prediction, which has potential applications in various fields, such as biomedical sensing and environmental monitoring. Comparing the simulation results with SDA, a commonly used analysis technique, validates the accuracy of the simulated transfer characteristics. However, a slight discrepancy in the output characteristics, specifically in the drain saturation current value, suggests that further refinement may be necessary for the model or simulation setup to achieve a closer match to experimental observations. It is crucial to investigate the factors causing this disparity and explore potential improvements to enhance the accuracy of the output characteristics simulation

The findings regarding the resistor and capacitor values indicate their limited influence on the transfer and output characteristics, emphasizing that the MOSFET parameters play a more significant role in shaping the device behavior. This underscores the importance of accurately characterizing and modeling the MOSFET parameters, such as width, length, transconductance, and threshold voltage, to ensure reliable simulation results.

Furthermore, incorporating the additional voltage, V_{SB}, in the modified equivalent circuit demonstrates its ability to produce varying V_T values corresponding to different pH levels, like what is observed in experimental results. This highlights the effectiveness of the proposed modification in capturing the influence of pH on the device's behavior.

5.1Limitations

The accuracy of the electrochemical equivalent circuit largely depends on the circuit components' accuracy and values. Therefore, the experimental values used to obtain these component values may be unclear, affecting the quality of the simulation findings. On the other hand, the electrochemical equivalent circuit is a simplified representation of the complex electrochemical processes that occur in the pH sensor. It is based on linear behavior and ignores various nonlinearities and interdependencies between components. This simplification may result in discrepancies between the simulated and actual sensor responses.

A complete list of abbreviations is shown in *Appendix I.*

6.Conclusion and future work

This study successfully simulated the EGFET equivalent circuits using LTSPICE XVII with discrete components. The research employs precise modeling and simulation techniques that have significant potential in forecasting the output current in relation to varying pH levels. The findings indicate that the simulation graph of transfer characteristics corresponds closely to the SDA, although there is a slight difference in the output characteristic graph, particularly in the value of the drain saturation current. The transfer and output characteristics of the equivalent circuit were found to be minimally affected by the values of the resistor and capacitor. However, the MOSFET parameters, including width, length, transconductance, and threshold voltage, were crucial in determining the device's behavior. Moreover, the inclusion of the modified equivalent circuit with an additional voltage, V_{SB}, successfully generated varying V_T values corresponding to different pH levels, aligning with experimental findings. In addition, the accuracy of the simulated transfer characteristics was validated by comparing the simulation results with the commonly used SDA analysis technique. There appears to be a minor inconsistency in the output characteristics, specifically in the value of the drain saturation current. It can be concluded that additional model or simulation setup improvements are necessary to achieve a more accurate alignment with experimental observations. Thus, future work may conduct a sensitivity analysis on the MOSFET parameters such as width, length, transconductance, and threshold voltage. Systematically varying these parameters within a reasonable range and observing the resulting changes in the transfer and output characteristics could help to identify the most influential parameters and fine-tune the values to enhance accuracy and reliability.

Acknowledgment

This study was partially supported by the Ministry of Higher Education Malaysia under Fundamental Research Grant Scheme under the (Project Code: FRGS/1/2021/TK0/UITM/02/50).

Conflicts of interest

The authors have no conflicts of interest to declare.

Author's contribution statement

Shaiful Bakhtiar Hashim: Design circuit, simulation, data collection, writing original draft and editing. **Muhammad Alhadi Zulkefle:** Carried out the experiment and data collection. **Zurita Zulkifli:** Anchored the review, revisions, and approved the article submission. **Sukreen Hana Herman:** Conceptualized the central research idea, and provided the theoretical framework.

The older version of this paper is already available on Research Square Preprint, with the following DOI: https://doi.org/10.21203/rs.3.rs-1031896/v1.

References

[1] Bouhoun ML, Blondeau P, Louafi Y, Andrade FJ. A paper-based potentiometric platform for determination of water hardness. Chemosensors. 2021; 9(5):1-12.

[2] Singewald TD, Traxler I, Schimo-Aichhorn G, Hild S, Valtiner M. Versatile, low-cost, non-toxic potentiometric pH-sensors based on niobium. Sensing and Bio-Sensing Research. 2022; 35:100478.

[3] Chen F, Yang Q, Jiang M, Meng Y, Zhang DW, Wang J. Visualization of electrochemical reactions on microelectrodes using light-addressable potentiometric sensor imaging. Analytica Chimica Acta. 2022; 1224:340237.

[4] Kagilev AA, Morozov VI, Zueva EM, Gafurov ZN, Mikhailov IK, Kantyukov AO, et al. Electrochemical behaviour of 2, 2′-bibenzimidazoles: Voltammetric, in situ UV–vis-and EPR-spectroelectrochemical and computational studies. Journal of Electroanalytical Chemistry. 2022; 921:116669.

[5] Kaur S, Shiekh BA, Kumar V, Kaur I. Triazole-tethered naphthalimide-ferrocenyl-chalcone based voltammetric and potentiometric sensors for selective electrochemical quantification of Copper (II) ions. Journal of Electroanalytical Chemistry. 2022; 905:115966.

[6] Park J, Song H, Choi H. Estimation of water-to-cement ratio in cementitious materials using electrochemical impedance spectroscopy and artificial neural networks. Construction and Building Materials. 2022; 350:128843.

[7] Havigh MD, Wouters B, Hallemans N, Claessens R, Lataire J, Terryn H, et al. Operando odd random phase electrochemical impedance spectroscopy for in situ

monitoring of the anodizing process. Electrochemistry Communications. 2022; 137:1-5.
[8] Singh M, Patkar R, Vinchurkar M, Baghini MS. Voltammetry based handheld measurement system for soil pH. Journal of Electroanalytical Chemistry. 2021; 885:1-8.
[9] McCormick WJ, Robertson PK, Skillen N, McCrudden D. The first electrochemical evaluation and voltammetric detection of the insecticide emamectin benzoate using an unmodified boron-doped diamond electrode. Results in Chemistry. 2023; 5:100865.
[10] Lee CS, Kim SK, Kim M. Ion-sensitive field-effect transistor for biological sensing. Sensors. 2009; 9(9):7111-31.
[11] Rosli AB, Awang Z, Shariffudin SS, Herman SH. Annealing temperature dependence of ZnO nanostructures grown by facile chemical bath deposition for EGFET pH sensors. In IOP conference series: materials science and engineering 2018 (pp. 1-7). IOP Publishing.
[12] Lauks I, Chan P, Babic D. The extended gate chemically sensitive field effect transistor as multi-species microprobe. Sensors and Actuators. 1983; 4:291-8.
[13] Chiang JL, Jhan SS, Hsieh SC, Huang AL. Hydrogen ion sensors based on indium tin oxide thin film using radio frequency sputtering system. Thin Solid Films. 2009; 517(17):4805-9.
[14] Chiu YS, Tseng CY, Lee CT. Nanostructured EGFET pH sensors with surface-passivated ZnO thin-film and nanorod array. IEEE Sensors Journal. 2011; 12(5):930-4.
[15] Wang CW, Pan TM. Structural properties and sensing performances of CoNxOy ceramic films for EGFET pH sensors. Ceramics International. 2021; 47(18):25440-8.
[16] Pan TM, Wang CW, Weng WC, Lai CC, Lu YY, Wang CY, et al. Rapid and label-free detection of the troponin in human serum by a TiN-based extended-gate field-effect transistor biosensor. Biosensors and Bioelectronics. 2022; 201:113977.
[17] Yang CC, Chen KY, Su YK. TiO_2 nano flowers based EGFET sensor for pH sensing. Coatings. 2019; 9(4):1-7.
[18] Ohshiro K, Sasaki Y, Minami T. An extended-gate-type organic transistor-based enzymatic sensor for dopamine detection in human urine. Talanta Open. 2023; 7:1-6.
[19] Mello HJ, Mulato M. Well-established materials in microelectronic devices systems for differential-mode extended-gate field effect transistor chemical sensors. Microelectronic Engineering. 2016; 160:73-80.
[20] Wang X, Jin C, Eshraghian JK, Iu HH, Ha C. A behavioral spice model of a binarized memristor for digital logic implementation. Circuits, Systems, and Signal Processing. 2021; 40:2682-93.
[21] Hunde BR, Woldeyohannes AD. Future prospects of computer-aided design (CAD)–a review from the perspective of artificial intelligence (AI), extended reality, and 3D printing. Results in Engineering. 2022:1-9.
[22] Leppänen J. Methodology, applications and performance of the CAD-based geometry type in the serpent 2 Monte Carlo code. Annals of Nuclear Energy. 2022; 176:1-10.
[23] Vidal FP, Mitchell IT, Létang JM. Use of fast realistic simulations on GPU to extract CAD models from microtomographic data in the presence of strong CT artefacts. Precision Engineering. 2022; 74:110-25.
[24] Martinoia S, Grattarola M, Massobrio G. Modelling non-ideal behaviours in H+-sensitive FETs with SPICE. Sensors and Actuators B: Chemical. 1992; 7(1-3):561-4.
[25] Martinoia S, Massobrio G. A behavioral macromodel of the ISFET in SPICE. Sensors and Actuators B: Chemical. 2000; 62(3):182-9.
[26] Abu Samah NL, Lee KY, Jarmin R. H+-ion-sensitive FET macromodel in LTSPICE IV. Journal of Computational Electronics. 2016; 15(4):1407-15.
[27] Kwon DW, Kim S, Lee R, Mo HS, Kim DH, Park BG. Macro modeling of ion sensitive field effect transistor with current drift. Sensors and Actuators B: Chemical. 2017; 249:564-70.
[28] Das A, Wang HT. pH-sensitive ultra-thin oxide liquid metal system. arXiv preprint arXiv:2007.09843. 2020.
[29] Hussin MR, Ismail R, Syono I. Simulation and fabrication of extended gate ion sensitive field effect transistor for biosensor application. In computer applications for security, control and system engineering: international conferences, SecTech, CA, CES 3 2012, Held in Conjunction with GST 2012, Jeju Island, Korea. Proceedings 2012 (pp. 396-403). Springer Berlin Heidelberg.
[30] Viton-Zorrilla L, Lezama J. A software platform for ISFET simulation based on open source tools to fit model parameters. In XXVI international conference on electronics, electrical engineering and computing 2019 (pp. 1-4). IEEE.
[31] Sinha S, Mukhiya R, Sharma R, Khanna PK, Khanna VK. Fabrication, characterization and electrochemical simulation of AlN-gate ISFET pH sensor. Journal of Materials Science: Materials in Electronics. 2019; 30:7163-74.
[32] Dinar AM, Zain AM, Salehuddin F, Attiah ML, Abdulhameed MK. Modeling and simulation of electrolyte pH change in conventional ISFET using commercial Silvaco TCAD. In IOP Conference series: materials science and engineering 2019 (p. 042020). IOP Publishing.
[33] Sinha S, Sahu N, Bhardwaj R, Ahuja H, Sharma R, Mukhiya R, Shekhar C. Modeling and simulation of temporal and temperature drift for the development of an accurate ISFET SPICE macromodel. Journal of Computational Electronics. 2020; 19(1):367-86.
[34] Archbold G, Parra C, Carrillo H, Mouazen AM. Towards the implementation of ISFET sensors for in-situ and real-time chemical analyses in soils: a practical review. Computers and Electronics in Agriculture. 2023; 209.

[35] Sinha S, Bhardwaj R, Sahu N, Ahuja H, Sharma R, Mukhiya R. Temperature and temporal drift compensation for Al_2O_3-gate ISFET-based pH sensor using machine learning techniques. Microelectronics Journal. 2020; 97:1-16.
[36] Tayeb AM, Solyman AA, Hassan M, el-Ella TM. Modeling and simulation of dye-sensitized solar cell: model verification for different semiconductors and dyes. Alexandria Engineering Journal. 2022; 61(12):9249-60.
[37] Patella B, Narayan T, O'Sullivan B, Daly R, Zanca C, Lovera P, Inguanta R, O'Riordan A. Simultaneous detection of copper and mercury in water samples using in-situ pH control with electrochemical stripping techniques. Electrochimica Acta. 2023; 439:141668.
[38] Shojaei Baghini M, Vilouras A, Douthwaite M, Georgiou P, Dahiya R. Ultra-thin ISFET-based sensing systems. Electrochemical Science Advances. 2022; 2(6):e2100202.
[39] Dhar R, Kumar N, Garcia CP, Georgiev V. Assessing the effect of scaling high-aspect-ratio ISFET with physical model interface for nano-biosensing application. Solid-State Electronics. 2022; 195:108374.
[40] Gaddour A, Dghais W, Hamdi B, Ben Ali M. Temperature compensation circuit for ISFET sensor. Journal of Low Power Electronics and Applications. 2020; 10(1):1-16.
[41] Thakur HR, Dutta JC. Modeling of carbon nanotube ISFETs with high-κ gate dielectrics for biosensing applications. International Journal of Numerical Modelling: Electronic Networks, Devices and Fields. 2019; 32(6):1-13.
[42] Chen CH, Liu SB, Chang SP. Fabrication and characterization of In0. 9Ga0. 1O EGFET pH sensors. Coatings. 2021; 11(8):1-9.
[43] Vidal-Iglesias FJ, Solla-Gullón J, Rodes A, Herrero E, Aldaz A. Understanding the Nernst equation and other electrochemical concepts: an easy experimental approach for students. Journal of Chemical Education. 2012; 89(7):936-9.
[44] Gualandi I, Tessarolo M, Mariani F, Tonelli D, Fraboni B, Scavetta E. Organic electrochemical transistors as versatile analytical potentiometric sensors. Frontiers in Bioengineering and Biotechnology. 2019; 7:354.
[45] Nascimento RA, Mulato M. Mechanisms of ion detection for FET-sensors using FTO: Role of cleaning process, pH sequence and electrical resistivity. Materials Research. 2017; 20:1369-79.
[46] Kumar A. Effect of body biasing over CMOS inverter. Threshold. 2013; 1:3.

Shaiful Bakhtiar Hashim received his Diploma in Electrical Electronics from Universiti Teknologi MARA in 2007. He received B. Eng and MSc degrees in Electrical Engineering from Universiti Teknologi MARA (UiTM) Shah Alam, Malaysia in 2009 and 2014, respectively. Later, he bocome a lecturer at UiTM Cawangan Terengganu. He is currently pursuing his Ph. D. degree at UiTM Shah Alam. His research interest includes the Fabrication and Characterization Of Semiconductor Materials in general and Nanostructured Materials.
Email: shaifulbakhtiar@uitm.edu.my

Zurita Zulkifli received her Diploma in Electronic Engineering from Universiti Teknologi Malaysia Kuala Lumpur in 2000. She received her B.Eng in Electrical Engineering from Universiti Teknologi MARA (UiTM), Shah Alam, Malaysia in 2004 and received her MSc in Microelectronics from Universiti Kebangsaan Malaysia in 2007. She received her Doctor of Engineering (Frontier Materials) in 2015 from Nagoya Institute of Technology, Japan. Currently, she serves as a senior lecturer at the School of Electrical Engineering, UiTM Shah Alam. Her research interests include Circuit Development, Fabrication and characterization of Semiconductor Materials and exploring the Graphene and Metal-Oxide Composite films for various applications.
Email: zurita101@uitm.edu.my

Muhammad AlHadi Zulkefle received his BSc. (Hons) degree in Materials Technology and MSc. degree in Electrical Engineering from Universiti Teknologi MARA, Shah Alam, Selangor, Malaysia, in 2014 and 2018 respectively. He is currently pursuing Ph.D. degree in Electrical Engineering at the same university. From 2014 to 2022, he worked as a Research Assistant with the Integrated Sensors Research Group. His research interests include the Fabrication of Micro and Nanostructured Materials (using equipment such as spin coating, dip coating, sputtering, hydrothermal immersion, electrospinning and electrospraying), for implementation in Solid-State pH Sensors.
Email: alhadizulkefle@gmail.com

Sukreen Hana Herman received her Ph.D. (Materials Science) in 2009 from the Japan Advanced Institute of Science and Technology (JAIST). Sukreen was with Sharp-Roxy before pursuing her Master. She joined Universiti Teknologi MARA (UiTM) in 2004 and now is the senior lecturer at the School of Electrical Engineering, College of Engineering UiTM. She is a member of the Integrated Sensor Research group at the College of Engineering. Her research interests include Fabrication and Characterization of Semiconductor Materials in general an mainly focused on Sensor Applications. Sukreen is one of the authors for more than 170 indexed articles and conference proceedings.
Email:hana1617@uitm.edu.my

Appendix I

S. No.	Abbreviation	Description
1	BJT	Bipolar Junction Transistors
2	CAD	Computer-Aided Design
3	EGFET	Extended-Gate Field Effect Transistor
4	FET	Field Effect Transistor
5	I_D	Drain Current
6	ISE	Ion-Selective Electrodes
7	ISFET	Ion-Sensitive Field Effect Transistor
8	MOSFET	Metal Oxide Semiconductor Field-Effect Transistor
9	NMOS	N-type Metal Oxide Semiconductor
10	PDI	Potential Determining Ions
11	PMOS	P-type Metal Oxide Semiconductor
12	RE	Reference Electrode
13	SDA	Semiconductor Device Analyzer
14	SE	Sensing Electrode
15	SPICE	Simulation Program with Integrated Circuit Emphasis
16	TiO_2	Titanium Dioxide
17	V_{DS}	Drain to Source Voltage
18	V_{GS}	Gate to Source Voltage
19	V_{REF}	Reference Voltage
20	V_T	Threshold Voltage